PROCEEDINGS OF SPIE

SPIEDigitalLibrary.org/conference-proceedings-of-spie

Comparative study of rare-earth doped low-phonon fluoride and chloride crystals for mid-IR laser potential

Brown, E., Fleischman, Z., McKay, J., Hömmerich, U., Trivedi, S., et al.

E. E. Brown, Z. D. Fleischman, J. McKay, U. Hömmerich, S. B. Trivedi, M. Dubinskii, "Comparative study of rare-earth doped low-phonon fluoride and chloride crystals for mid-IR laser potential," Proc. SPIE 11724, Laser Technology for Defense and Security XVI, 117240C (12 April 2021); doi: 10.1117/12.2587796



Event: SPIE Defense + Commercial Sensing, 2021, Online Only

Comparative study of rare-earth doped low-phonon fluoride and chloride crystals for mid-IR laser potential

E. E. Brown*a, Z. D. Fleischmana, J. McKaya, U. Hömmerichb, S.B. Trivedic, and M. Dubinskiia aUS Army Research Laboratory, ATTN FCDD-RLS-CL, 2800 Powder Mill Rd, Adelphi, MD, USA 20783-1138; b Dept. of Physics, Hampton University, Hampton, VA, USA 23668-0105; Brimrose Corporation of America, Sparks Glencoe, MD, USA 21152-2300

ABSTRACT

A comparative study was performed on the mid-infrared emission properties of trivalent erbium (Er³⁺) and holmium (Ho³⁺) doped fluorides (BaF₂, NaYF₄) and ternary chloride-based crystals (CsCdCl₃, KPb₂Cl₅,)- All crystals were grown by vertical Bridgman technique. Following optical excitation at 800 nm, all Er³⁺ doped fluorides and chlorides exhibited mid-infrared emissions at ~4500 nm at room temperature. The mid-infrared emission at 4500 nm, originating from the ${}^{4}I_{9/2} \rightarrow {}^{4}I_{11/2}$ transition, showed long emission lifetime values of ~11.6 ms and ~3.2 ms for Er³⁺ doped CsCdCl₃ and KPb₂Cl₅ crystals, respectively. In comparison, Er³⁺ doped and BaF₂ and NaYF₄ demonstrated rather short lifetimes in the microsecond range of ~47 μs and ~205 μs, respectively. Temperature dependent decay time measurements were performed for the ⁴I_{9/2} excited state for Er³⁺ doped BaF₂, NaYF₄, and CsCdCl₃ crystals. We noticed that the emission lifetimes of Er3+:CsCdCl3 were nearly independent of the temperature, whereas significant emission quenching of 4I9/2 level was observed for both Er3+ doped fluoride crystals. The temperature dependence of the multiphonon relaxation rate for 4.5 μm mid-IR emissions was determined for the studied Er³⁺ doped fluorides using the well-known energy-gap law. Using ~890 nm excitation, all studied Ho³⁺ doped fluorides and chlorides exhibited mid-infrared emissions at ~3900 nm originating from the ${}^5I_5 \rightarrow {}^5I_6$ transition. The longest emission lifetime of the 5I_5 level was determined to be ${\sim}14.55$ ms from the Ho³⁺:CsCdCl₃ crystal. The room temperature stimulated emission cross-sections for the Er³⁺ ${}^{4}I_{9/2} \rightarrow {}^{4}I_{11/2}$ and $\text{Ho}^{3+5}\text{I}_5 \rightarrow {}^5\text{I}_6$ transitions were determined using the Füchtbauer-Landenburg equation. Among the studied crystals, Er^{3+} doped chlorides are more than two orders of magnitude better in terms of emission lifetimes and sigma-tau product than the fluoride crystals.

Keywords: rare earth ions, erbium, holmium, mid-infrared, chlorides, fluorides, solid-state lasers

1. INTRODUCTION

There has been much recent interest in solid-state lasers emitting in the mid-IR spectral region (3-5 µm) due to a wide array of applications including remote sensing of bio-chemical agents, free-space communications, molecular spectroscopy, and medical procedures [1-17]. Rare-earth (RE) ions such as Er³+, Ho³+, Pr³+, Dy³+, Nd³+, Tb³+, and Tm³+ have gained significant attention for their rich emission transitions in the 3-5 µm spectral region [1-17]. However, achieving laser operation at longer infrared (IR) wavelengths is difficult in traditional oxide laser hosts since RE ions suffer from large non-radiative decay rates through multi-phonon relaxation (MPR). The main barrier is to find the proper laser materials with the right dopant and host combination to obtain efficient mid-IR emission at room temperature, and also to have suitable pumping scheme. Over the recent years, studies in mid-IR lasing have focused on the low maximum phonon energy materials for good reason: because this aspect is required for minimizing the nonradiative rates through MPR [3-17].

In this work, we report a comparative spectroscopic characterization between RE³⁺ (Er³⁺, Ho³⁺) doped fluorides and chlorides. The representative materials for fluorides were BaF₂ and NaYF₄. In the fluorite family, BaF₂ is one of the laser hosts of interest due to its low maximum energy and high thermal conductivity [18]. Studies of visible and upconversion luminescence spectroscopy of RE doped BaF₂ materials were reported [19-21]; however, very little studies were performed for the mid-IR spectral region [16,17]. Very recently, the author reported the 4.5 μm fluorescence properties of Er³⁺ doped BaF₂ single crystal for potential mid-IR laser sources [16]. RE doped NaYF₄,in the form of powders, nanoparticles, ceramics, and glasses, has been widely studied with respect to its upconversion characteristics [22-24].

Laser Technology for Defense and Security XVI, edited by Mark Dubinskii, Lawrence Grimes, Proc. of SPIE Vol. 11724, 117240C ⋅ © 2021 SPIE CCC code: 0277-786X/21/\$21 ⋅ doi: 10.1117/12.2587796

Representative ternary chloride crystals studied here include cesium cadmium chloride (CsCdCl₃) and potassium lead chloride (KPb₂Cl₅). RE doped CsCdCl₃ (CCC) materials have not been studied for their mid-infrared emission properties; so far their attention has been mainly towards applications in optoelectronics and scintillators [25-29]. KPb₂Cl₅ (KPC) has already demonstrated lasing from the incorporation of several RE dopants including Er:KPC at 1.7 μ m and 4.5 μ m [3,4], Dy:KPC at 2.4 μ m [12], and Nd:KPC at 1.06 μ m [12]. In this paper, results of the spectroscopic investigations of the 4.5 μ m and 3.9 μ m emission properties of Er³⁺ and Ho³⁺ doped fluorides and chlorides crystals are presented, respectively.

2. EXPERIMENTAL CONSIDERATIONS

The investigated BaF_2 and $NaYF_4$ materials crystallize in the cubic structure with wide band gaps and wide transparency ranges of 0.2-14 µm and 0.15-11 µm, respectively [16,17,21-24]. The studied chloride crystals such as CCC crystallize in the cubic perovskite structure [26] whereas KPC is a monoclinic crystal [3,4]. They all have low maximum phonon energies between 200 and 400 cm⁻¹ [3,4,16,21,25]. The physical properties of all studied crystals, including their corresponding maximum phonon energies are listed in Table 1. CCC has a low moisture sensitivity while KPC is considered non-hygroscopic. RE^{3+} (Er^{3+} , Ho^{3+}) doped BaF_2 and $NaYF_4$ crystals were grown by Bridgman technique. RE^{3+} (Er^{3+} , Ho^{3+}) doped CCC and KPC crystals were grown at Hampton University using a two-zone crystal growth furnace by Bridgman technique. Details of the material preparation and crystal growth process were expressed elsewhere [15,17]. The Er^{3+} and Ho^{3+} concentrations in the studied samples ranged between 1.5 and 2 x 10^{20} cm⁻³.

Room temperature absorption spectra were recorded using a Cary 6000i UV-Vis-NIR spectrophotometer. Mid-IR emission spectra were recorded after excitation with a continuous-wave Spectra-Physics Tsunami Ti:Sapphire laser. A Princeton Instruments Acton Spectra-Pro 0.15 m monochromator (λ_{blaze} : 4 μ m, 150 grooves/mm) was used to collect the mid-IR fluorescence spectra. The emission signal was recorded by an Infrared Associates liquid-nitrogen-cooled InSb

Table 1. Physical characteristics of studied fluoride and ternary-based chloride crystals.

Property	BaF ₂ NaYF ₄ [16,17,21,30] [22-24]		CsCdCl ₃ (CCC)	KPb ₂ Cl ₅ (KPC)
Crystal structure	Cubic	Cubic	Cubic perovskite	Monoclinic
Transparency Range (μm)	0.3 - 14	0.15 - 11	0.3 - 15	0.3 - 20
Melting point (°C)	820	780	553	434
Density (g/cm³)	4.89	4.20	3.86	4.63
Band gap (eV)	~ 6.6	~ 8.0	~ 4.76	~ 3.77
Refractive index	~1.47	~1.475	~1.72 [29]	~1.95 [3,4]
Maximal phonon energy (cm ⁻¹)	324	~ 360	~ 252 [25]	203 [3,4]
Robustness	Chemically Rugged	Rugged	Low moisture sensitivity	Non- hygroscopic

detector in conjunction with a Stanford Research Systems SR830 dual-phase lock-in amplifier. Fluorescence decay measurements were carried out using the output of a pulsed (10 ns pulses, 10 Hz) Nd:YAG pumped Optical Parametric

^{*}eiei.brown.civ@mail.mil; phone 1 301 394-2293; fax 1 301 394-0310

Oscillator (OPO) system. The emission decay transients were recorded with a LabView-driven National Instruments data acquisition system. For temperature dependence fluorescence studies, the sample was mounted on the cold finger of a two-stage closed-cycle helium refrigerator.

3. RESULTS AND DISCUSSION

3.1. Er3+ doped fluorides and chlorides

Figure 1(a) shows the room temperature ground state absorption spectra of Er³⁺ doped BaF₂, NaYF₄, CCC, and KPC crystals in the near-IR (700-1800 nm) region. All the absorption spectra were corrected for background absorption due to Fresnel and other parasitic effects. All studied crystals showed light pink color (except for Er³⁺:CCC) with successful Er³⁺ incorporation. As can be seen in the images of the as-grown boules and cut pieces of the studied crystals (Fig. 1(a)), Er³⁺:BaF₂ exhibited good optical quality whereas the Er³⁺:NaYF₄ boule was largely cloudy and only a few transparent pieces could be extracted for spectroscopy. For the investigated chloride materials, a good quality Er³⁺ doped KPC crystal was cut from the boule whereas, for Er³⁺ doped CCC, only a low transparency and polycrystalline sample was available. Despite having similar Er³⁺ concentrations in these crystals, Er³⁺ doped fluoride crystals have slightly stronger absorption than the chlorides in the diode-pumped region (800 nm and 980 nm). A partial energy level diagram indicating the corresponding absorption lines from the ground state ⁴I_{15/2} is illustrated in Fig. 1(b).

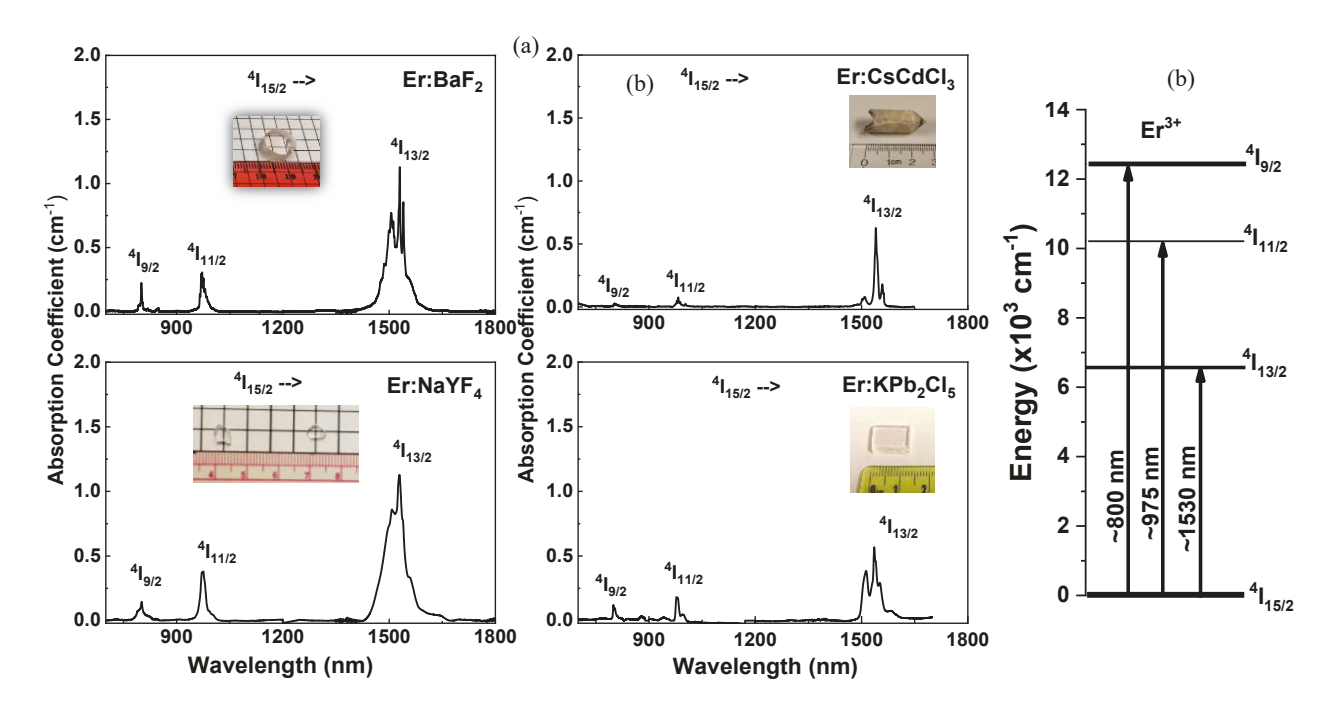


Figure 1. Room temperature absorption spectra of (a) Er^{3+} : BaF_2 and Er^{3+} : $NaYF_4$, Er^{3+} : $CsCdCl_3$ and Er^{3+} : KPb_2Cl_5 crystals. (b) A partial energy level diagram showing the corresponding absorption lines from the ground state $^4I_{15/2}$.

Using the absorption data, Judd-Ofelt (J-O) analysis was performed for the studied Er^{3+} doped fluoride crystals. A J-O calculation was not performed for Er^{3+} :CCC due to poor quality of the investigated sample. Additional purification and crystal growth experiments of Er: CCC are in progress and will be reported in an upcoming manuscript. Table 2 lists the J-O intensity parameters of the Er^{3+} :BaF₂, Er^{3+} :NaYF₄, and Er^{3+} :KPC crystals [13,16,21]. These J-O parameters are in reasonable agreement with other reported values for Er^{3+} :BaF₂ [21] and Er^{3+} :NaYF₄ [23]. The mid-IR transition of interest in this work is the Er^{3+} 4.5 µm fluorescence arising from the ${}^4I_{9/2} \rightarrow {}^4I_{11/2}$ transition. Table 3 shows the calculated radiative transition rates, branching ratios, and radiative lifetimes of the ${}^4I_{9/2}$ excited state. It can be noted that the energy spacing between the ${}^4I_{9/2}$ and ${}^4I_{11/2}$ manifolds is about 2200 cm⁻¹ (Fig. 1(b)), and hence, the branching ratios for this energy gap are typically small, between 1 and 2 % (Table 3). The normalized mid-IR emission spectra (${}^4I_{9/2} \rightarrow {}^4I_{11/2}$) of

Table 2. Judd-Ofelt intensity parameters of Er:BaF2, Er:NaYF4, and Er:KPb2Cl5.

Crystals	Ω_2 (10 ⁻²⁰ cm ²)	Ω_4 (10 ⁻²⁰ cm ²)	Ω_6 (10 ⁻²⁰ cm ²)
Er:BaF2	1.98	1.18	1.20
Er:NaYF4	3.97	0.96	0.84
Er:KPb ₂ Cl ₅ [13]	0.385	1.099	0.898

Table 3. Calculated radiative rates, branching ratios, and radiative lifetime values of the ⁴I_{9/2} excited state for the investigated Er:BaF₂, Er:NaYF₄, and Er:KPb₂Cl₅ crystals.

Crystals	Transitions	(nm)	A _{ij} (s ⁻¹)	βij	τ _{rad} (ms)
Er:BaF ₂ [21]	$^{4}I_{9/2} \rightarrow ^{4}I_{11/2}$	4510	0.573	0.016	
	$^{4}I_{9/2} \rightarrow ^{4}I_{13/2}$	1700	34.94	0.365	
	$^{4}I_{9/2} \rightarrow ^{4}I_{15/2}$	802	59.227	0.619	10.45
Er:NaYF4	$^{4}I_{9/2} \rightarrow ^{4}I_{11/2}$	4520	0.36	0.005	
	$^{4}I_{9/2} \rightarrow ^{4}I_{13/2}$	1705	24.64	0.277	
	$^{4}I_{9/2} \rightarrow ^{4}I_{15/2}$	815	58.20	0.719	11.02
Er:KPb2Cl5 [13]	$^{4}I_{9/2} \rightarrow ^{4}I_{11/2}$	4490	3.22	0.013	
	$^{4}I_{9/2} \rightarrow ^{4}I_{13/2}$	1710	67.55	0.268	
	$^{4}I_{9/2} \rightarrow ^{4}I_{15/2}$	810	181.6	0.719	3.9

the studied $\rm Er^{3+}$ doped fluoride and chloride crystals obtained at room temperature under ~800 nm excitation are depicted in Fig. 2(a). Figure 2(b) shows a partial energy level diagram with the relevant transitions. Broad emission bands were centered ~4500 nm with a linewidth of ~ 325 nm ($\rm Er^{3+}:BaF_2$), ~350 nm ($\rm Er^{3+}:NaYF_4$), ~175 nm ($\rm Er^{3+}:CCC$), and ~270 nm ($\rm Er^{3+}:KPC$).

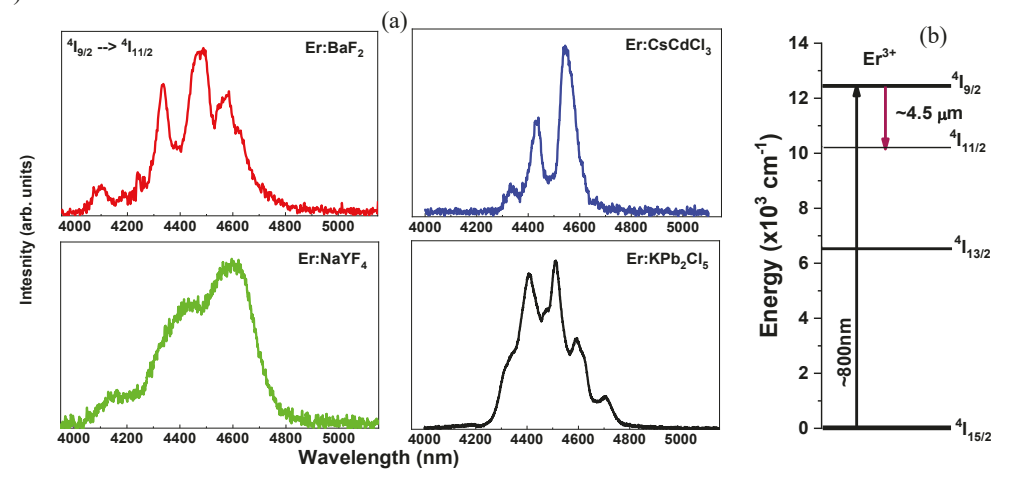


Figure 2. (a) Room temperature normalized mid-IR emission spectra of ${}^4I_{9/2} \rightarrow {}^4I_{11/2}$ transition in Er:BaF₂, Er:NaYF₄, Er:CsCdCl₃, and Er:KPb₂Cl₅ crystals. (b) The partial energy level diagram of Er³⁺ ions indicating the excitation wavelength and corresponding emission transition.

Figure 3 illustrates the room temperature ${}^4I_{9/2}$ emission decay transients under pulsed excitation at ${\sim}800$ nm. The most remarkable difference between Er³⁺ doped fluorides and chlorides is the large difference in the room temperature mid-IR emission lifetimes. Long emission lifetimes of ${\sim}11.6$ ms and ${\sim}3.2$ ms were observed from Er³⁺ doped CCC and KPC crystals, respectively. Meanwhile, Er³⁺ doped BaF₂ and NaYF₄ crystals demonstrated rather short lifetimes in the microsecond range, with values of ${\sim}47$ µs and ${\sim}205$ µs, respectively. These lifetime values follow the trend of chlorides

having much lower phonon energies than the fluorides, suggesting negligibly small nonradiative decay rates for the chloride hosts.

To gain more insight into the decay dynamics of the studied crystals, the temperature dependence of the 4.5 μ m decay time was measured from 10 K to 295 K for the Er³+BaF₂, Er³+:NaYF₄, and Er³+:CCC crystals (Fig. 4 (a)). For Er³+:CCC, the emission lifetimes were nearly constant across the whole temperature range, indicating that nonradiative decay processes are negligibly small. In contrast, for Er³+:BaF₂ and Er³+:NaYF₄, the lifetimes exhibited a significant increase with temperature, reaching values of ~125 μ s (not included in Fig. 4(a)) and ~590 μ s at 10 K, respectively. This corresponds to the emission lifetimes being quenched by ~62% and ~67% for the same temperature range, for these respective crystals. It is known that nonradiative decay can take place due to several possible processes including MPR, energy transfer between RE ions in different

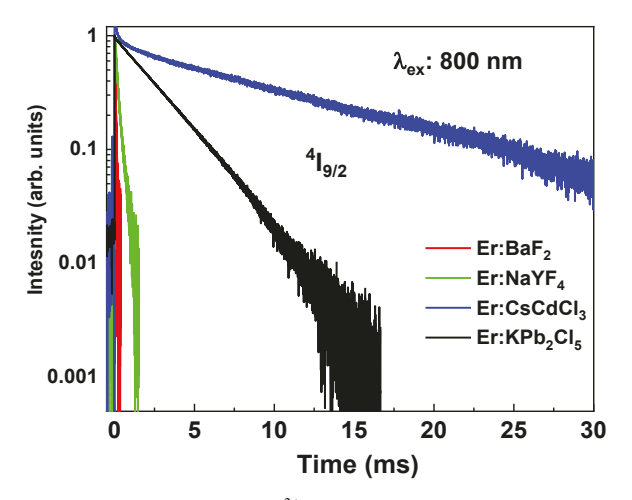


Figure 3. ${}^4I_{9/2}$ emission decay transients of the studied Er^{3+} doped fluoride and chloride crystals under 800 nm excitation at room temperature.

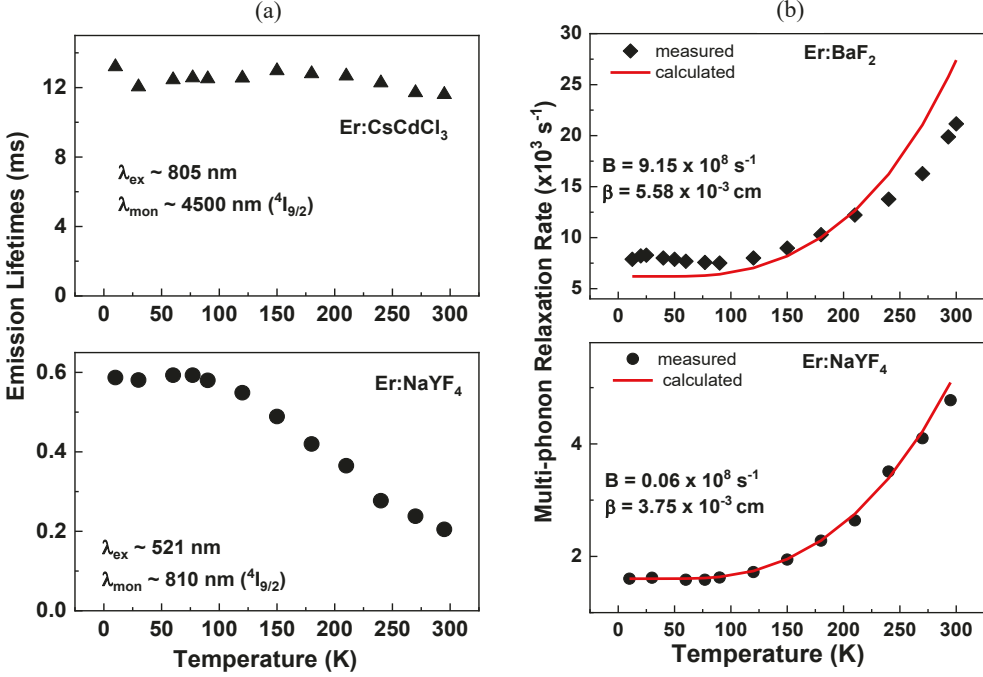


Figure 4. (a) Temperature dependence of the ⁴I_{9/2} level lifetime values between 10 K and room temperature for Er:CsCdCl₃ and Er:NaYF₄ crystals. (b) Exponential energy-gap law fitting of the ⁴I_{9/2} level for both Er:BaF₂ and Er:NaYF₄ crystals.

incorporation sites, and energy transfer to other impurities in the crystal [9,13,16,31,32]. Thus, the possibility of MPR as the cause for the observed 4.5 μ m emission quenching in Er³⁺ doped fluoride crystals was further explored. The energy-gap law, which describes the rate of nonradiative decay due to MPR (W_{MPR}) between rare-earth energy levels, is expressed by [2]:

$$W_{MPR} = Be^{-\beta\Delta E} \left[1 - e^{-(\hbar\omega/kT)}\right]^{-p} \tag{1}$$

where ΔE is the energy spacing of the transition, T is the temperature, $\hbar \omega$ is the maximum phonon energy of the host material, p is the number of phonons needed to bridge the energy gap, and B and β are both empirically derived host dependent parameters. The detailed calculation of host dependent fitting parameters (B = 9.15 x 10^8 s⁻¹ and β = 5.58 x 10⁻³ cm) for Er³⁺:BaF₂ was described by the author previously [16]. A similar approach was performed for Er³⁺:NaYF₄ crystals, which resulted in B = 0.06 x 10^8 s⁻¹ and β = 3.75 x 10^{-3} cm. Figure 4(b) depicts the comparison of the experimentally derived nonradiative decay rates to the theoretical MPR based on the energy-gap law. It was found that the MPR rates do not match up between the experimental and modeled values, as a function of temperature, for the Er³⁺:BaF₂ crystal. It can be seen that there are some contributions of MPR, which suggest that other nonradiative decay processes are active in the crystal. Another complication in Er: BaF₂ is the existences of multiple Er³⁺ sites which can further complicate the de-excitation dynamics of Er³⁺ ions [16]. Studies have shown that there can be asignificant number of Er³⁺ clustering sites in BaF₂ even at a very low concentration of less than 0.1 % [31]. On the contrary, for Er³⁺:NaYF₄ the change in lifetime with temperature is consistent with multiphonon decay as described by energy-gap law. Based on the measured emission lifetimes and the calculated radiative lifetimes (from J-O analysis) listed in Table 4, the quantum efficiency of 4.5 μ m (${}^{4}I_{9/2} \rightarrow {}^{4}I_{11/2}$) emissions in Er³⁺:BaF₂ and Er³⁺:NaYF₄ were determined to ~0.4 % and ~2.1 %, respectively. In contrast, for Er³⁺:KPC it can be concluded that the emission quantum efficiency is near unity at all temperatures. As mentioned earlier, the calculated radiative lifetime for Er³⁺:CCC is not available at present. However, the maximum lifetime value, from temperature dependent emission lifetimes recorded between 10 K and room temperature, was assumed as the radiative lifetime (\sim 13.0 ms) of the $^4I_{9/2} \rightarrow ^4I_{11/2}$ transition, which yielded a quantum efficiency of ~89 %.

Table 4. Room temperature (experimental), radiative lifetimes, and quantum efficiencies of ${}^4I_{9/2} \rightarrow {}^4I_{11/2}$ transition for the investigated Er³⁺ doped BaF₂, NaYF₄, CsCdCl₃, and KPb₂Cl₅ crystals. * Maximum lifetime value assumed as radiative lifetime for Er³⁺:CCC.

Crystal	τ _{300K} (ms)	τ _{rad} (ms)	η _{QE} (%)
Er:BaF2	0.047	10.45	~ 0.4
Er:NaYF4	0.205	11.02	~ 2.1
Er:CsCdCl3	11.6	13.0*	~ 89
Er:KPb2Cl5	3.2	3.9	~ 100

The emission cross-section of the ${}^4I_{9/2} \rightarrow {}^4I_{11/2}$ mid-IR transition was calculated using the Füchtbauer-Landenburg (F-L) equation [33]:

$$\sigma_{emiss}(\lambda) = \frac{\beta \lambda^5 I(\lambda)}{8\pi n^2 c \, \tau_{rad} \int \lambda I(\lambda) d\lambda} \tag{2}$$

where β and τ_{rad} are the branching ratio of the 4500 nm emission and the radiative lifetime of the transition upper level, respectively. $I(\lambda)$ is the emission intensity at wavelength λ and n is the refractive index of the host. The room temperature stimulated emission cross-section spectra of all studied Er^{3+} doped fluoride and chloride crystals are depicted in Fig. 5(a), while Fig. 5(b) displays the partial energy level diagram of Er^{3+} ions indicating the emission transition of interest ${}^4I_{9/2} \rightarrow {}^4I_{11/2}$. Table 5 lists the peak emission cross-sections, emission lifetimes, and the σ - τ product of the studied crystals. It was observed that the peak emission cross-sections for Er doped fluorides and chlorides showed similar values. The σ - τ product (where σ is the stimulated emission cross-section and τ is the upper laser level lifetime)

is typically considered a good figure of merit for lasers since its value is inversely proportional to the laser threshold under continuous wave excitation. Thus, the larger the σ - τ product, the lower the threshold pump power. It is noted that the values σ - τ product for Er^{3+} doped chlorides are two orders of magnitude larger than the Er^{3+} doped fluorides. It is suggested that longer lifetimes in the chlorides resulted in lower laser threshold than in the fluorides.

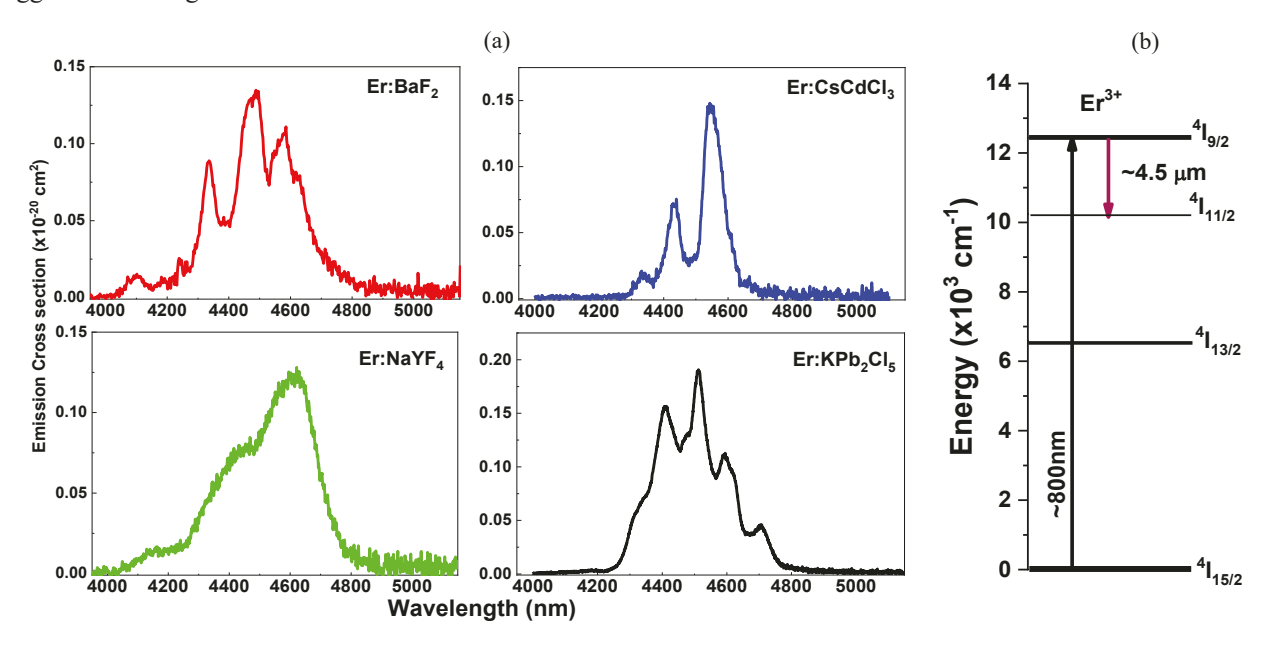


Figure 5. (a) Stimulated emission cross-sections for the ${}^4I_{9/2} \rightarrow {}^4I_{11/2}$ transition in the investigated Er³⁺ doped fluoride and chloride crystals at room temperature, which were calculated using the Füchtbauer-Landenburg equation. (b) The partial energy level diagram of Er³⁺ ions indicating the emission transition of interest ${}^4I_{9/2} \rightarrow {}^4I_{11/2}$.

Table 5. Experimental lifetimes, emission cross-sections, and sigma-tau product for the ⁴I_{9/2} excited state for all studied four Er³⁺ doped fluoride and chloride crystals.

Crystal	λ _{peak} (nm)	$\begin{array}{c} \sigma_{em}(\lambda) \\ (10^{-20} cm^2) \end{array}$	τ _{300K} (ms)	σ-τ (10 ⁻⁰ cm ² .ms)
Er:BaF2	~4495	~ 0.13	0.047	0.006
Er:NaYF4	~4562	~ 0.12	0.205	0.025
Er:CsCdCl3	~4545	~ 0.14	11.6	1.62
Er:KPb2Cl5	~4510	~ 0.18	3.2	0.58

3.2. Ho³⁺ doped fluorides and chlorides

The room temperature infrared absorption spectra spanning from 700 nm to 2300 nm of $Ho^{3+}:BaF_2$, $Ho^{3+}:NaYF_4$, and $Ho^{3+}:KPb_2Cl_5$ are shown in Fig. 6(a). The characteristic absorption bands were assigned to transitions from the 5I_8 ground sate to the excited states of the Ho^{3+} ion. A partial energy level diagram indicating the corresponding absorption lines from the ground state 5I_8 is illustrated in Fig. 6(b). The absorption spectrum of the synthesized polycrystalline $Ho^{3+}:CCC$ sample is not currently available. All the presented absorption spectra were corrected for background absorption due to Fresnel and other parasitic effects. As can be seen in the images of the cut pieces of the studied Ho^{3+} doped crystals (Fig. 6(a)), $Ho^{3+}:BaF_2$ was of good optical quality, whereas $Ho^{3+}:NaYF_4$ was rather milky in some parts of the boule resulting in only a few transparent pieces suitable for transmission studies. We attained a good quality and highly transparent Ho^{3+} doped KPC sample with a light pink coloration. It is known that the absorption of the 5I_5 level is

typically weak in $\mathrm{Ho^{3+}}$ doped materials as can also be seen in the studied $\mathrm{Ho^{3+}}$ doped crystals. The absorption coefficients of the ${}^{5}\mathrm{I}_{5}$ excited state are found to be \sim 0.054 (@892 nm), 0.082 (@890.5 nm), and 0.065 (@891.5 nm) cm⁻¹

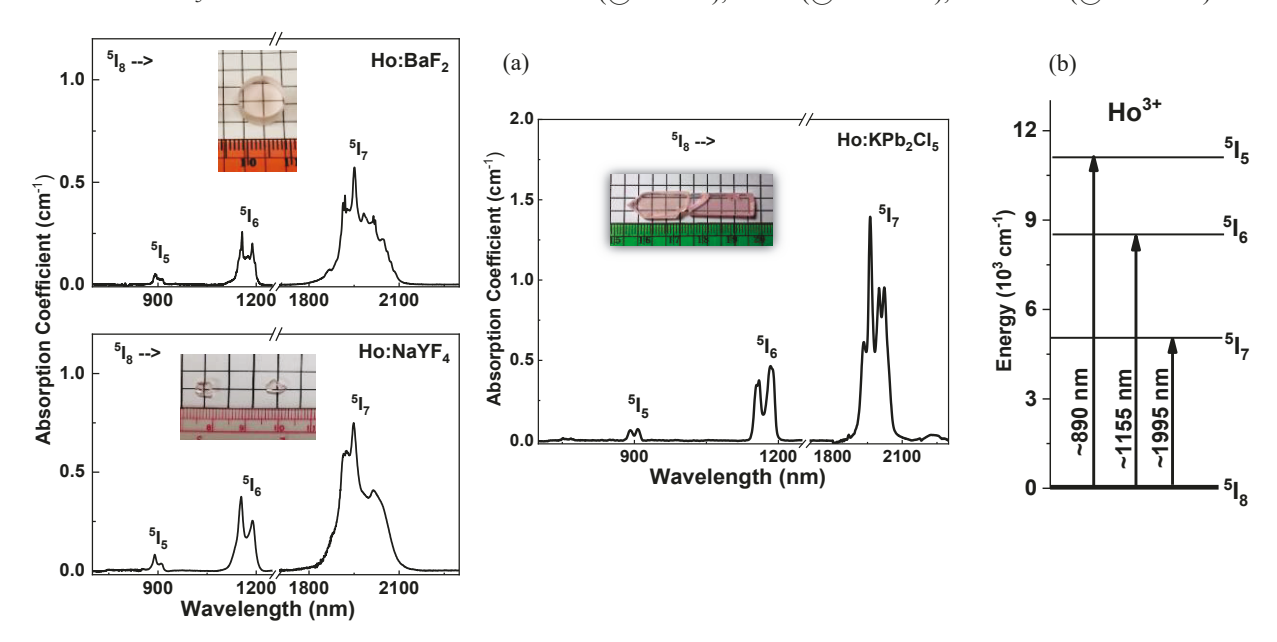


Figure 6. Room temperature absorption spectra of (a) $\mathrm{Ho^{3+}:BaF_2}$, $\mathrm{Ho^{3+}:NaYF_4}$, and $\mathrm{Ho^{3+}:KPb_2Cl_5}$ crystals. (b) An energy level diagram showing the corresponding absorption lines from the ground state ${}^5\mathrm{I}_8$.

for the Ho³⁺:BaF₂, Ho³⁺:NaYF₄, and Ho³⁺:KPC crystals, respectively. Not only is the 5I_5 level (~890 nm) of great importance for laser diode pumping, but it also is the resonant excitation for the mid-IR emission at 3900 nm. Figure 7(a) displays the room temperature normalized mid-IR emission spectra (${}^5I_5 \rightarrow {}^5I_6$) of the studied Ho³⁺ doped fluoride and chloride crystals acquired under ~890 nm excitation. A partial energy level diagram of Ho³⁺ ions, indicating the excitation wavelength and observed emission transition, is illustrated in Fig. 7(b). We observed mid-IR emission bands

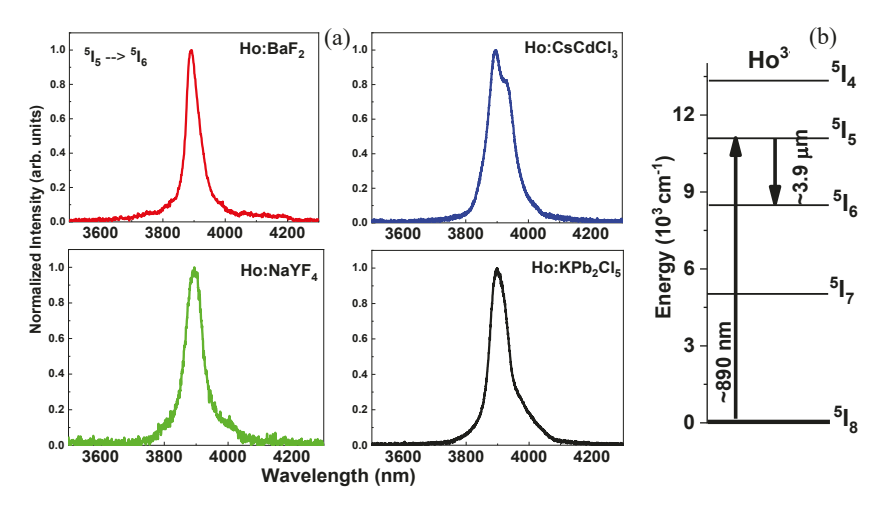


Figure 7. (a) Room temperature mid-IR emission spectra of the studied Ho³⁺ doped fluorides and chlorides centered at ~ 3900 nm (${}^{5}I_{5} \rightarrow {}^{5}I_{6}$). (b) The partial energy level diagram of Ho³⁺ ions indicating the emission transition of interest ${}^{5}I_{5} \rightarrow {}^{5}I_{6}$.

centered \sim 3900 nm with a linewidth of \sim 53 nm (Ho³⁺:BaF₂), \sim 61 nm (Ho³⁺:NaYF₄), \sim 90 nm (Ho³⁺:CCC), and \sim 70 nm (Ho³⁺:KPC). The enhancement of 3900 nm emission from Ho³⁺ via Tm³⁺ sensitization has been reported in BaF₂ [17]. To the best of our knowledge, the mid-IR emission (3900 nm) of Ho³⁺:NaYF₄ has not been reported in literature.

Figure 8 exhibits the room temperature 5I_5 emission decay transients of all studied Ho³⁺ doped crystals under pulsed excitation at ~890 nm. As was the case for Er³⁺ doped crystals, the 5I_5 Ho³⁺ emission lifetimes are relatively long with a value of ~14.55 ms for Ho³⁺:CCC and ~5 ms for Ho³⁺:KPC crystals. Virey et al. [14] reported mid-IR fluorescence of ~3.9 μ m for Ho³⁺ doped CsCdBr₃ with the emission lifetime of 13 ms for 5I_5 level, which has the similar value to the studied Ho³⁺:CCC crystal. In contrast, the lifetime values of Ho³⁺ doped BaF₂ and NaYF₄ crystals were significantly shorter, in the microsecond range of ~22 μ s and ~ 120 μ s, respectively. It can be noted that the reported emission lifetimes for the 5I_5 level in Ho³⁺:YLF and Ho³⁺:BYF crystals are also in the microsecond range of ~18 μ s and ~50 μ s, respectively [1].

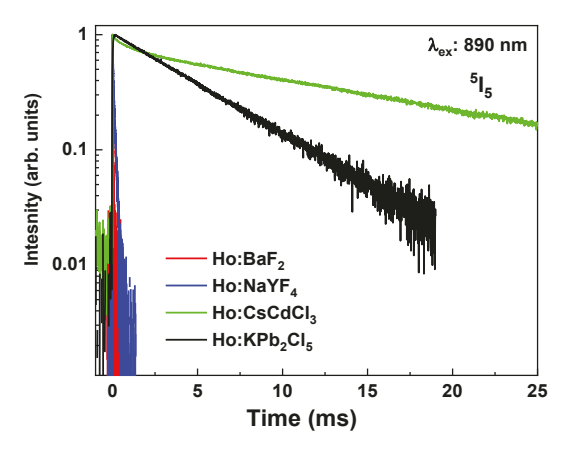


Figure 8. ${}^{5}I_{5}$ emission decay transients of the studied Ho $^{3+}$ doped fluoride and chloride crystals under 890 nm excitation at room temperature.

The room temperature stimulated emission cross-sections of all studied Ho³⁺ doped fluoride and chloride crystals were calculated using F-L method (Eq. 2), and are shown in Figure 9. The calculated radiative lifetimes for Ho³⁺:BaF₂ Ho³⁺:NaYF₄ and Ho³⁺:KPC are determined to be 10.2 ms [34], 9.87 ms [22], and 4 ms [15], respectively. Since the radiative lifetime for Ho³⁺:CCC is not avaliable at present, the experimental lifetime of the 5 I₅ level (~14.55 ms) is applied to estimate the value of emission cross-section. The peak emission cross-sections are determined to be ~0.61 x 10^{-20} , ~0.62 x 10^{-20} , ~0.44 x 10^{-20} , and ~1.4 x 10^{-20} cm² for Ho³⁺:BaF₂ Ho³⁺:NaYF₄, Ho³⁺:CCC, and Ho³⁺:KPC, respectively. Due to the large difference in emission lifetimes, the obtained σ - τ product for the Ho³⁺ doped chlorides is almost three orders of magnitude larger than the similarly doped fluorides. More detailed studies on J-O analysis, temperature dependent spectra, and decay dynamics of Ho³⁺ doped fluoride and chloride crystals will be reported in an upcoming manuscript.

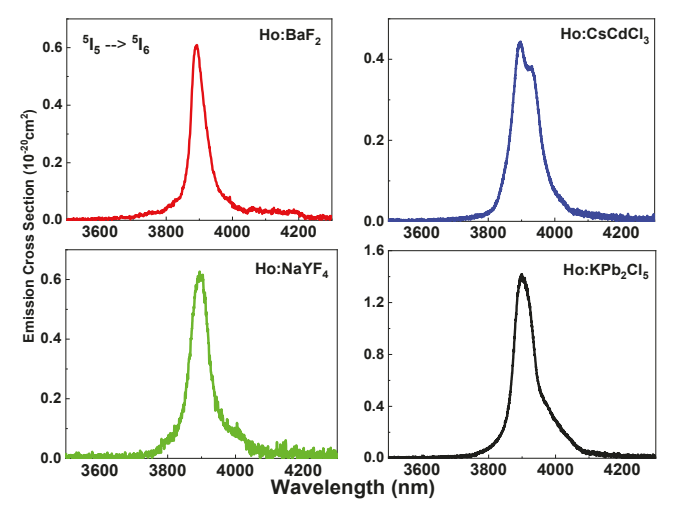


Figure 9. Stimulated emission cross-section for the ${}^5I_5 \rightarrow {}^5I_6$ transition in all investigated Ho³⁺ doped fluorides and chlorides at room temperature, which were calculated using the Füchtbauer-Landenburg equation.

4. SUMMARY AND CONCLUSIONS

Comparative mid-IR spectroscopic studies of Er^{3+} and Ho^{3+} doped fluorides and ternary-based chloride crystals grown by Bridgman technique were presented. All investigated crystals exhibited fluorescence in the attractive mid-infrared region from 3 to 5 µm region. Mid-infrared fluorescence properties at room temperature, as well as at cryogenic temperatures, were explored. Broad mid-IR emission bands centered at ~4500 nm ($^4I_{9/2} \rightarrow ^4I_{11/2}$) of Er^{3+} and ~3900 nm ($^5I_5 \rightarrow ^5I_6$) of Ho^{3+} were observed for all studied Er^{3+} and Ho^{3+} doped crystals under ~800 nm and ~890 nm excitations, respectively. The peak mid-IR emission cross-sections of the Er^{3+} $^4I_{9/2} \rightarrow ^4I_{11/2}$ transition were determined to be between 0.14 - 0.18 x $^{10-20}$ cm² whereas values between 0.44 - 1.4 x $^{10-20}$ cm² were found for the Ho^{3+} $^5I_5 \rightarrow ^5I_6$ transition. Overall, the chloride host materials demonstrated superior spectroscopic results in terms of emission lifetimes and σ - τ product compared to the fluorides. However, chlorides present significant challenges in terms of crystal growth, low thermal conductivity, and mechanical strength. Fluoride crystals can be grown with higher optical quality, though strong mid-IR emission quenching can lead to higher laser threshold and poor overall laser efficiency. Moreover, fluorides do offer superior thermal and mechanical properties compared to the chlorides. To conclude, materials optimization studies will continue on Er^{3+} and Ho^{3+} doped low maximum phonon energy crystals to demonstrate mid-IR lasing in the 3-5 µm region.

ACKNOWLEDGEMENTS

The work at Hampton University was supported by the National Science Foundation through grant NSF-DMR 1827820 (PREM) and the Army Research Office through grant W911NF1810447.

REFERENCES

- [1] Eichhorn, M., "Quasi-three-level solid-state lasers in the near and mid infrared based on trivalent rare earth ions," Appl Phys B. 93, 269-316 (2008).
- [2] Kaminskii, A.A., Crystalline lasers: physical processes and operating schemes. Boca Raton (FL): CRC Press (1996).
- [3] Velazquez, M., Ferrier, A., Doualan, J.-L. and Moncorge, R. "Rare-earth doped low phonon energy halide crystals for mid-infrared sources," in: A. Al-Khursan, editor. Solid-State Laser. London (UK): IntechOpen; pp. 119-142 (2012).
- [4] Bowman, S.R., Searles, S.K., Jenkins, N.W., Qadri, S.B., Skelton, E.F. and Ganem, J., "Diode pumped room temperature mid-infrared erbium laser," In: Marshall C, editor. Advanced Solid-State Lasers. Washington (DC): Optical Society of America; OSA trends in optics and photonics Vol. 50, 154–156 (2001).
- [5] Brown, E., Fleischman, Z., Merkle, L. D., Rowe, E., Burger, A., Payne, S. A. and Dubinskii M., "Optical spectroscopy of holmium doped K₂LaCl₅," J Lumin. 196, 221-226 (2018).
- [6] Orlovskii, Y.V., Basiev, T.T., Pukhov, K.K., Doroshenko, M.E., Badikov, V.V., Badikov, D.V., Alimov, O.K., Polyachenkova, M.V., Dmitruk, L.N., Osiko, V.V. and Mirov, S.B., "Mid-IR transitions of trivalent neodymium in low phonon laser crystals," Opt. Mater. 29, 1115-1128 (2007).
- [7] Okhrimchuk, A.G., Butvina, L.N., Dianov, E.M., Shestakova, I.A., Lichkova, N.V., Zagorodnev, V.N. and Shestakov, A.V., "Optical spectroscopy of the RbPb₂Cl₅:Dy³⁺ laser crystal and oscillation at 5.5 μm at room temperature," J. Opt. Soc. Am. B 24, 2690-2695 (2007).
- [8] Bowman, S.R., Shaw, L.B., Feldman, B.J. and Ganem, J., "A 7-μm praseodymium-based solid-state laser," IEEE J. Quantum Electron. 32, 646-649 (1996).
- [9] Brown, E., Hanley, C.B., Hommerich, U., Bluiett, A.G. and Trivedi, S.B. Trivedi, "Spectroscopic study of neodymium doped potassium lead bromide for mid-infrared solid state lasers," J. Lumin. 133, 244-248 (2013).
- [10] Jelinkova, H., Doroshenko, M.E., Jelinek, M., Sulc, J., Osiko, V.V., Badikov, V.V. and Badikov, D.V., "Dysprosium-doped PbGa₂S₄ laser generating at 4.3 μm directly pumped by 1.7 μm laser diode," Opt. Lett. 38, 3040-3043 (2013).
- [11] Nostrand, M.C., Page, R.H., Payne, S.A., Schunemann, P.G. and Isaenko, L.I., "Laser demonstrations of rare-earth ions in low phonon chloride and sulfide crystals," in: H. Lasers, U. Injeyan, Keller, C. Marshall (Eds.), Advanced

- Solid State Lasers, OSA Topics in Optics and Photonics Series (Optical Society of America, Washington, D.C., Vol. 34, 459–463 (2000).
- [12] Jenkins, N.W., Bowman, S.B. Bowman, O'Connor, S., Searles, S.K. and Ganem, J., "Spectroscopic characterization of Er-doped KPb₂Cl₅ laser crystals," Opt. Mater. 22, 311-320 (2003).
- [13] Virey, E., Couchaud, M., Faure, C., Ferrand, B. Wyon, C. and Borel, C., "Room temperature fluorescence of CsCdBr₃:RE (RE = Pr, Nd, Dy, Ho, Er, Tm) in the 3 5 µm range," J. Alloys Compd. 275-277, 311-314 (1998).
- [14] Oyebola, O., Hommerich, U., Brown, E., Trivedi, S.B., Bluiett, A.G., Zavada, J.M., "Growth and optical spectroscopy of Ho-doped KPb₂Cl₅ for infrared solid-state lasers," J. Cryst. Growth 312, 1154-1156 (2010).
- [15] Brown, E.E., Fleischman, Z., McKay, J., Dubinskii M., "Spectroscopic characterization of low-phonon Er-doped BaF₂ single crystal for mid-IR lasers," Opt. Mater. Exp. 11(2), 575-584 (2021).
- [16] Orlovskii, Yu.V., Basiev, B.B., Pukhov, K.K., Alimov, O.K., Glushkov, N.A., Konyushkin, V.A., "Low-phonon BaF₂:Ho³⁺,Tm³⁺ doped crystals for 3.5-4 µm lasing," Opt. Mater. 31, 599-611 (2010).
- [17] Brown, E.E., Fleischman, Z., Hawrami, R., Ariesanti, E., Burger, A., Hommerich, U., Trivedi, S.B., Dubinskii M., "Mid-IR emission characteristics of low-phonon erbium-doped ternary chloride-based single crystals," Proc. SPIE 11682, 11682R-1-9 (2021).
- [18] Popov, P.A., Fedorov, P.P., Osiko, V.V., "Thermal conductivity of single crystals with a fluorite structure: Cadmium Fluoride," Phys. Solid State 52(3), 504-508 (2010).
- [19] Chen, X., Wu, Y., "High concentration Ce³⁺ doped BaF₂ transparent ceramics," J. Alloys Cmpd. 817, 153075 (1-6) (2020).
- [20] Chen, G., Xiao, H., Man, S.Q., Zhang, J.Q., Ren, S.X., "Radiation damage of rare earth ions doped barium fluoride crystals," Supercollider 4, 809-815 (1992).
- [21] Bitam, A., Khiari, S., Diaf, M., Boubekri, H., Boulma, E., Bensalem, C., Guerbous, L., Jouart, J.P., "Spectroscopic investigation of Er³⁺ doped BaF₂ single crystal," Opt. Mater. 82, 104-109 (2018).
- [22] Yang, S., Haiping, X., Zhang, J., Jiang, Y., Shi, Y., Gu., X., Zhang, J., Zhang, Y., Jiang, H., Chen, B., "Growth and spectral properties of Ho³⁺ doped α-NaYF₄ single crystal," Opt. Mater. 45, 209-214 (2015).
- [23] Wang, C., Xia, H., Feng, Z., Zhang, Z., Jiang, D., Zhang, J., He, S., Tang, Q., Sheng, Q., Gu, X., Zhang, Y., Chen, B., Jiang, H., Infrared spectral properties for α-NaYF₄ single crystal of various Er³⁺ doping concentrations," Opt. Lsr. Tech. 82, 157-162 (2016).
- [24] Ojha, N., Tuomisto, M., Lastusaari, M., Petit, L., "Upconversion from fluorophosphates glasses prepared with NaYF₄:Er³⁺, Yb³⁺ nanocrystals," RSC Adv. 8, 19226-19236 (2018).
- [25] Demirbilek, R., Feile, R., and Bozdogan, C., "Temperature dependent Raman spectra of CsCdBr₃ and CsCdCl₃ crystals," J. Lumin. 161, 174-179 (2015).
- [26] Romanov, A.N., Veber, A.A., Fattakhova, T., Vtyurina, D.N., Kouznetsov, M., Sulimov, V.B., "Spectral properties and NIR photoluminescence of Bi⁺ impurity in CsCdCl₃ ternary chloride," J. Lumin. 149, 292-296 (2014).
- [27] Hommerich, U., Uba, S., Kabir, A., Trivedi, S.B., Yang, C. and Brown, E., "Visible emission studies of melt-grown Dy-doped CsPbCl₃ and KPb₂Cl₅ crystals," Opt. Mater. Exp. 10(8), 2011-2018 (2020).
- [28] Kobayashi, M., Omata, K., Sugimoto, S., Tamagawa, Y., Kuroiwa, T., Asada, H., Takeuchi, T. and Kondo, S., "Scintillation characteristics of CsPbCl₃ single crystals," Nucl. Instrum. Methods Phys. Res., Sect. A 592(3), 369-373 (2008).
- [29] Ghebouli, B., Ghebouli, M.A., Fatmi, M. and Bouhemadou, "First-principles study of the structural, elastic, electronic, optical and thermodynamic properties of the cubic perovskite CsCdCl₃ under high pressure," Solid St. Comm. 150, 1896-1901 (2010).
- [30] Richman, I., "Longitudinal optical phonons in CaF₂, SrF₂, and BaF₂," J. Chem. Phys. 41(9), 2836-2837 (1964).
- [31] Miller, M. and Wright, J.C., "Single site multiphonon and energy transfer relaxation phenomena in BaF₂:Er³⁺," J. Chem. Phys. 68(4), 1548-1562 (1978).
- [32] Andeen, C.G., Fontanella, J.J., Wintergill, M.C., Welcher, P.J., Kimble Jr, R.J., Matthews Jr, G.E., Clustering in rare-earth-doped alkaline earth fluorides," J. Phys. C: Solid State Phys. 14(24), 3557-3574 (1981).
- [33] Aull, B.F. and Jenssen, H.P., "Vibronic interactions in Nd:YAG resulting in nonreciprocity of absorption and stimulated emission cross sections," IEEE Quantum Electron. 18, 2559-2562 (2017).
- [34] Brown, E.E., McKay, J., Fleischman, Z., Merkle, L., Dubinskii M., "Optical characterization of rare-earth doped BaF₂ crystals for mid-IR laser sources," SPIE Photonics West, Optical Components and Materials XVI, paper 10914-79 (2019).